Space Weather

RESEARCH ARTICLE
10.1029/2018SW001872

Special Section:
Space Weather Events of 4-10 September 2017

Flares at Earth and Mars: An Ionospheric Escape Mechanism?

M. Mendillo[1], P. J. Erickson[2], S.-R. Zhang[2], M. Mayyasi[1], C. Narvaez[1], E. Thiemann[3], P. Chamberlain[3], L. Andersson[3], and W. Peterson[3]

[1]Center for Space Physics, Boston University, Boston, MA, USA, [2]Haystack Observatory, Massachusetts Institute of Technology, Westford, MA, USA, [3]Laboratory for Atmospheric and Space Physics, University of Colorado, Boulder, CO, USA

Key Points:
- Observations and models for Earth show that flare-induced ionospheric enhancements of N_e and T_e lead quickly to plasma escape
- September 2017 flares confirm terrestrial pattern at early times (~10 min), but observations at Mars only available after ~2 hr
- For Mars, analytical 1-D model predicts upward plasma drift capable of escape; new observations for "early time" flare effects needed

Supporting Information:
- Supporting Information S1

Correspondence to:
C. Narvaez,
cnarvaez@bu.edu

Citation:
Mendillo, M., Erickson, P. J., Zhang, S.-R., Mayyasi, M., Narvaez, C., Thiemann, E., et al. (2018). Flares at Earth and Mars: An ionospheric escape mechanism? *Space Weather*, *16*, 1042–1056. https://doi.org/10.1029/2018SW001872

Received 28 MAR 2018
Accepted 30 JUN 2018
Accepted article online 13 JUL 2018
Published online 18 AUG 2018

Abstract Solar flares are nature's active experiment upon a planet's upper atmosphere and ionosphere. Observed effects at Earth are consistent with a "second sunrise" scenario that produces changes in electron density, electron temperature, and plasma dynamics. A solar active region in September 2017 provoked ionospheric disturbances due to solar flares observed at Earth (6 September) and later at Mars (10 and 17 September). Incoherent scatter radar observations from the Millstone Hill Observatory showed a burst of upward diffusion due to electron temperature enhancements. We explore the companion possibility of flares causing upward drifts and plasma escape at Mars. Solar observations made by the EUV Monitor instrument on the Mars Atmosphere and Volatile EvolutioN (MAVEN) satellite are used to portray the time histories of irradiance changes to determine the "early" (onset to peak emission) and "late" (decay to background) time scales for these flares. During the initial phase of a flare (when photons ionize an atmosphere unmodified by flare heating), MAVEN was well above the ionosphere and thus no in situ data are available to asses this period of possible plasma escape. Estimates made using a simple terrestrial model for plasma drifts in the topside ionosphere suggest that escape rates can be enhanced at Mars at "early" times. The "late time" effects observed below 400 km 2 hr after the flare onset times did not reveal conclusive remnants of the proposed mechanism. No model of the Martian thermosphere-ionosphere system has produced a self-consistent simulation of solar flare effects upon Mars' upper atmosphere and ionosphere.

1. Introduction

Planets with atmospheres are remarkably diverse (Catling & Kasting, 2017). Within our solar system, giant planets have their original atmospheres of hydrogen and helium (Jupiter, Saturn, Uranus, and Neptune), while the smaller planets have either secondary atmospheres of carbon dioxide, nitrogen, and oxygen (Venus, Earth, and Mars) or no permanent atmosphere (Mercury). While the escape of the primordial light-element atmospheres of the terrestrial planets was totally efficient, the relatively high gravity of Venus and Earth led to retention of their robust secondary atmospheres of heavier gases. The thin atmosphere currently found at Mars is the exception, and understanding that case study is one of the major goals of solar system science.

The study of escaping atmospheres deals with the transport of both neutrals and plasmas (Schunk & Nagy, 2009). An enormous literature exists on both topics using diverse terminologies (e.g., outflows, escape fluxes, beams, and plumes). The many drivers of escape range from internal conditions (e.g., temperature) to external forces (e.g., solar wind). To our knowledge, no study has considered solar flare effects upon an atmosphere as causing a distinct mode of escape. That is the topic of this paper. Our focus is on Mars, yet guided by previous studies of flare effects at Earth.

A very brief summary of prior work on the ionized component of escape at Mars begins with results from the Russian Phobus-2 mission (Lundin et al., 1989), followed by the many studies using the European Space Agency's Mars Express data sets (Barabash et al., 2007; Dubinin et al., 2009; Fränz et al., 2010; Lundin et al., 2008, 2009; Nilsson et al., 2010, 2011; Ramstad et al., 2013, and references therein). The global escape rates for electrons and ions found in all of these prior studies consistently fell within the range of ~10^{24} to ~10^{25} per second.

National Aeronautics and Space Administration (NASA) MAVEN mission strives to quantify the current escape processes for neutral and ionized gases at Mars and to use them to estimate long-term atmospheric loss (Jakosky, 2015). Plasma escape rates found using MAVEN observations are also in ~10^{24} to ~10^{25}/s range. Brain et al. (2015) estimated a lower bound value of 3×10^{24}/s for ions with energies >25 eV observed

beyond the ionosphere (but originating in the ionosphere, $h < 400$ km). Jakosky et al. (2015) combined observations and modeling to arrive at a rate of ~1.5×10^{24} ions/s for low solar wind conditions. Mendillo, Narvaez, Vogt, et al. (2017) used changes in total electron content (TEC) to quantify the portion of the topside ionosphere lost during ionopause lowering events caused by changing solar wind conditions. They estimated a global loss rate of ~3×10^{24} ions/s. In all of these cases, the cause of plasma escape was attributed to ambient or enhanced solar wind effects, namely, "pick-up" or "stripping" of the ions and electrons in the topside ionosphere of Mars. Dong et al. (2015) note that on average about one fourth of the O^+ escaping flux comes from the north polar region in the Mars-Sun-electric field coordinate system.

From a comparative ionosphere perspective, at Earth the outflow of O^+-rich plasma also occurs but through different acceleration mechanisms characteristic of cusp and high-latitude processes. The numerical values of aggregate ionospheric escape rates are about an order of magnitude larger, with the destination for ionospheric plasma being the magnetosphere. For example, the DE-1 spacecraft found total accelerated (10 eV–10+ keV) ion outflow rates of 4–5 $\times 10^{25}$ ions/s at quiet magnetic times regardless of solar activity (Yau et al., 1985). Strangeway et al. (2005, 2010) derived outflow scaling laws based on observations of cusp-region outflows at 4,000 km altitude, using data from the Fast Auroral Snapshot Explorer, and reached these same net flux values. During geomagnetic storms, the magnetosphere plasma of ionospheric origin escapes via plasmoid motion down the tail, and sometimes a portion is dynamically lost at the magnetopause boundary. Moreover, storm-time escape rates via E × B driven advection of cold plasma to cusp outflow regions in the ionosphere can reach considerably larger values $>10^{26}$ ions/s. This is a sufficient rate of plasma motion to redistribute a 1-Earth radius shell of the outer plasmasphere toward the dayside magnetopause (Foster et al., 2004).

In this study, we explore a hitherto unexplored mechanism for ionospheric escape at Mars—one that might occur following a solar flare. The increases in ionospheric densities due to a sudden enhancement of extreme ultraviolet (EUV) radiation ionizing neutrals above the altitude of maximum electron density (h_{max}) offer a new population of ions and electrons to escape by vertical plasma diffusion and/or "pick-up" by solar wind magnetic fields and plasma flow. We approach this mechanism by studying flare induced plasma dynamics at Earth where powerful ground-based diagnostics capture the physical processes operating, and then we apply those findings to Mars. There are no evolutionary consequences to "Earth-as-a-planet" due to flare-induced escape or to seasonally dependent escape rates (Peterson et al., 2001). At Mars, however, escape fluxes ten to a hundred times smaller have certainly affected the global Martian environment (Jakosky et al., 2015). The Earth's thermosphere and ionosphere are so robust that episodic escape of ionospheric plasma produced by a flare has no long-term implications. Can the same be said for Mars? With a far more tenuous atmosphere, low gravity, cold temperatures, and no global magnetic field, might flare-induced plasma escape from Mars' topside ionosphere have evolutionary consequences?

In section 2, we summarize the Haystack Observatory/Millstone Hill first-ever observations by an incoherent scatter radar (ISR) of plasma processes in the topside ionosphere ($h > h_{max}$) caused by a large solar flare at Earth. This was for the flare of 7 August 1972, as described in Mendillo and Evans (1974). The unanticipated result to emerge from that study was the prominent role of vertical plasma dynamics. In section 3, we describe why prior and subsequent flare effect observations by the ISR technique have been difficult to obtain. In section 4 we describe new ISR observations of flare-induced effects made on 6 September 2017. This event is of particular interest because it relates to the same solar active region that produced subsequent flares that affected the ionosphere at Mars 4 days later (10 September 2017), and again a week later (17 September 2017). In section 5, we conclude with a discussion of solar flares as a new source of ionospheric loss at Mars. Section 6 describes MAVEN's ionospheric observations on 10 and 17 September 2017, and section 7 gives a summary.

2. Prior Observations

2.1. Terrestrial Observing Methods

There are several main ways to observe enhancements in the Earth's ionosphere produced by solar flare photons: ground-based ionosondes, ISRs, cosmic radio absorption by the ionosphere (riometers), and satellite-to-ground radio methods. An ionosonde uses radio reflection methods in the HF band (3–30 MHz)

to observe electron densities at and below the altitude of maximum electron density (h_{max}). These include the maximum electron density of the *F* layer (N_mF_2) at *h* ~300 km, with a prominent secondary layer in the *E* layer (N_mE at *h* ~110 km). During a flare, the most energetic photons penetrate to the *D* layer ($h <$ ~80 km) to produce ionization that results in the absorption of radio waves from cosmic background sources as measured by riometers. In these situations, *D* layer absorption often causes the loss of ionosonde diagnostic information about the *E* and *F* layers early in the flare's temporal pattern (≤10–20 min).

Satellite radio beacon signals in the very high frequency (30–300 MHz) and ultrahigh frequency (0.3–3 GHz) range are usually unaffected by *D* layer absorption and thus can be used to measure TEC (TEC = $\int N_e(h)$ dh) during a flare. While TEC increases due to flares have been observed, specification of their altitude components is not possible from this information alone.

The most comprehensive ionospheric diagnostic uses very weak radar backscatter from electrons in the ionosphere, modified electrostatically by the presence of ions (Evans, 1969). Originally called the Thomson scatter technique, but with improved understanding of the physics, it is now called the ISR method. The benefit of the ISR observations is that the spectrum of the returned radar signal provides direct, quantitative, altitude-resolved information on profiles of electron density, ion composition, electron and ion temperatures, and plasma dynamics.

For temporal resolution, modern ionosondes provide data every 15 min (and often every 5 min). The worldwide Global Navigation Satellite System network, including the U.S. Global Positioning System (GPS), produces transionospheric TEC data on a minute-by-minute basis. Ionosondes and GPS systems operate continuously from many sites spanning the globe and thus flare effects are capable of being "routinely" observed. This is in marked contrast to results from ISR facilities that are resource-intensive to maintain and operate. Some of the large radars also have multiple users (e.g., radio and radar astronomy at the Arecibo Observatory), meaning observations must be time multiplexed. The restricted duty cycles for ISR observations result in considerably smaller ionospheric data coverage for rare events such as strong solar flares. For example, ISR observations at Millstone Hill routinely occur for approximately 1,000 hours per year (~3.5 days per month). Similar or slightly larger observing time for ionospheric monitoring occurs at the Arecibo Observatory, some of which is separately dedicated to coordinated international "world day" operations. Since flares are not predictable events for instrument scheduling purposes, there are remarkably few observations of ionospheric flare effects observed by ISR methods.

2.2. Studies of Solar Flare Effects Upon the Terrestrial Ionosphere

Ionosonde observing methods have operated for many decades on a global basis, and thus, case studies of flare effects upon the Earth's ionosphere also span many decades (Mitra, 1974). Prior to the Mendillo and Evans (1974) case study, however, only one previous report of flare effects observed by an ISR had been reported. Thome and Wagner (1971) used the ISR at the Arecibo Observatory to describe flares in May 1971. In that study, emphasis was given to heights below 240 km, with no reliable measures of electron densities or electron temperatures in the topside ionosphere. More recently, a similar emphasis upon the lower ionosphere occurred using simultaneous data sets from three ISRs (Millstone Hill, MA; Sondrestrom, Greenland; Tromso, Norway) for the flare of 7 September 2005 (Xiong et al., 2011). Thus, for both ISR and ionosonde methods (as recently emphasized by Handzo et al., 2014), virtually all prior observations of flare effects pertain to data from heights below the altitude of maximum electron density (h_{max}). This is where strong flare enhancements in X-rays produce proportionally larger effects upon the *E* layer (*h* ~110 km) than those caused by the EUV component of flare irradiance that modifies the *F* layer ($h >$ 200 km). Yet, with the overall electron density profile $N_e(h)$ capable of being affected by a flare, it is not surprising that the ionosphere's TEC has pronounced flare-induced enhancements (Garriott et al., 1967; Mendillo et al., 1974; Tsurutani et al., 2009).

Figure 1 presents the ISR profiles of electron density obtained during the solar flare event of 7 August 1972 by the ionospheric radar at Millstone Hill (42.6°N, 70.5°W). As anticipated from ionosonde studies, the flare's EUV produced smaller enhancements of electron density in the *F* layer ($h \geq h_{max}$) than those produced by X-rays in the *E* layer. Our emphasis here is upon the *F* layer where the change was +25% for N_{max} and +31% for TEC (with 14% below h_{max} and 42% above h_{max}). Figure 2 shows the results from the spectral analysis of the radar returns—altitude profiles of electron temperature (T_e), ion temperature (T_i), and bulk plasma drift (V_z). The

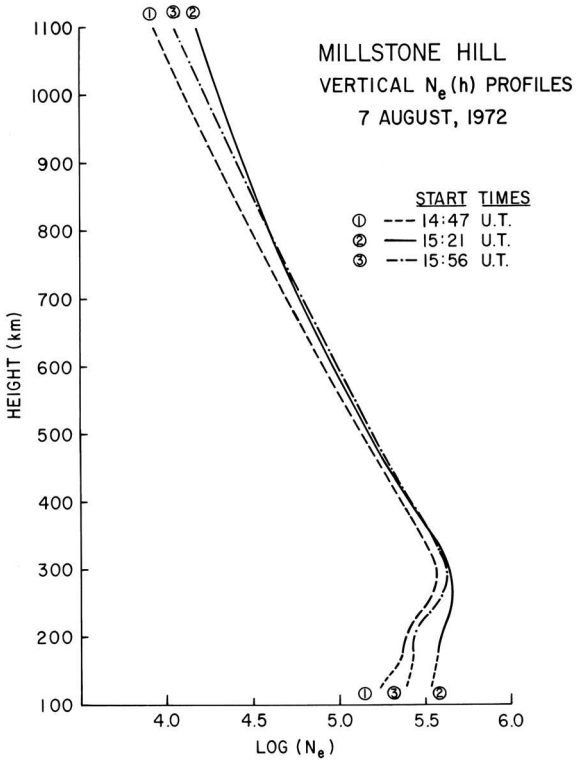

Figure 1. Observations of changes in the electron density profile on 7 August 1972 made by the Millstone Hill incoherent scatter radar (ISR). Solar radio flux observations at 35,000 MHz showed that a large solar flare occurred at 15:15 UT with peak emission at 15:22 UT (Mendillo et al., 1974).The ISR measurements shown refer to preflare, flaring, and postflare times, and electron density is given in cm^{-3}. Note that the largest changes in electron density occur in the lower ionosphere (*E* layer), with smaller changes at all altitude in the *F* layer (after Mendillo & Evans, 1974).

major result coming from this event was the surge in vertical plasma drift (V_z) shown in the right panel. Driven by the suddenly high electron temperatures (center panel) from the flare's photoelectron heating, the upward flux ($F = N_e \times V_z$) at 600 km is 4×10^{12} ion-electron pairs/m^2-s. The preflare value was zero flux at 600 km. Past studies of plasma fluxes are generally characterized as having upward values during the day and downward at night, with magnitudes of ~few $\times 10^{12}/m^2$ s (Banks & Kockarts, 1973; Evans, 1971; Schunk & Nagy, 2009). Global circulation models for the upper atmosphere, for example, TIME-GCM (Roble & Ridley, 1994), typically use such values for case studies of average morphologies (Rishbeth et al., 2009).

The event of 7 August 1972 was the first to associate a flare with a sudden and significant upward flux of plasma within the Earth's topside ionosphere. Even with a magnitude comparable to (or exceeding) typical daytime upward fluxes, there were no long-term consequences of significance. This is due to the strong confinement of ionospheric plasma exerted by the terrestrial geomagnetic field. An upward flux simply fills the vast regions called the plasmasphere—a donut-shaped domain extending to 4–6 earth-radii surrounding the Earth. There are episodes of erosion of that reservoir that occur during geomagnetic storms, when electrodynamics induced by changes in solar wind parameters result in the loss of plasma (Schunk & Nagy, 2009). Typically, recovery of the plasmaspheric reservoir occurs on time scales of ~days—driven by the normal daily ionization of the neutral atmosphere and upward diffusion of plasma (Sandel & Denton, 2007, and references therein).

2.3. Flare Studies at Mars

The first report of a solar flare effect at Mars was that by Gurnett et al. (2005) using the Mars Advanced Radar for Subsurface and Ionosphere Sounding (MARSIS) topside sounder radar on Mars Express. They found an enhancement of ~30% in the maximum electron density of the M2-layer (N_mM_2) as the response to an X1.1 flare on 15 September 2005—an effect that persisted for less than 7 min (Nielsen et al., 2006). A topside sounder (such as MARSIS) has no access to the electron density profiles below h_{max}, and thus, radio occultation studies were the first to show the dramatic, low-altitude effects within the Martian bottomside ionosphere (M1-layer) caused by the soft X-ray components of two solar flares (Mendillo et al., 2006). The event of 15 April 2001 was an X14.4 flare, and that of 26 April 2001 was an M7.8 flare. These case studies included simultaneous flare effect observations recorded by ionosondes at Earth. This first-ever two planet study of flares was made possible by the special geometry of Earth and Mars being nearly aligned with respect to the Sun (i.e., Mars was in opposition phase), and thus, the same solar irradiance enhancements impacted both planets.

Mahajan et al. (2009) offered confirmation of flare effects in the Mars Global Surveyor data base. Fallows et al. (2015) expanded on Mars in opposition-phase studies using 20 flares observed from Earth orbit during the years 2000–2005. Again using the Mars Global Surveyor data base of radio occultation profiles, Fallows et al. (2015) placed their emphasis on the M1-layer, offering a method to estimate flare-induced ionospheric enhancements.

The first studies of flare effects conducted using MAVEN instruments dealt with heating of the neutral atmosphere (Thiemann et al., 2015) and photoelectrons produced by flares (Peterson et al., 2016). We report here on the flare events of 6, 10, and 17 September 2017 to explore the situation of a single rotating solar active region provoking enhanced photon fluxes affecting two planets at widely separated orbital longitudes. In contrast to previous studies, we concentrate on the M2-layer and, in particular, at altitudes above the height of maximum electron density ($h > h_{max}$) where upward plasma flow is possible.

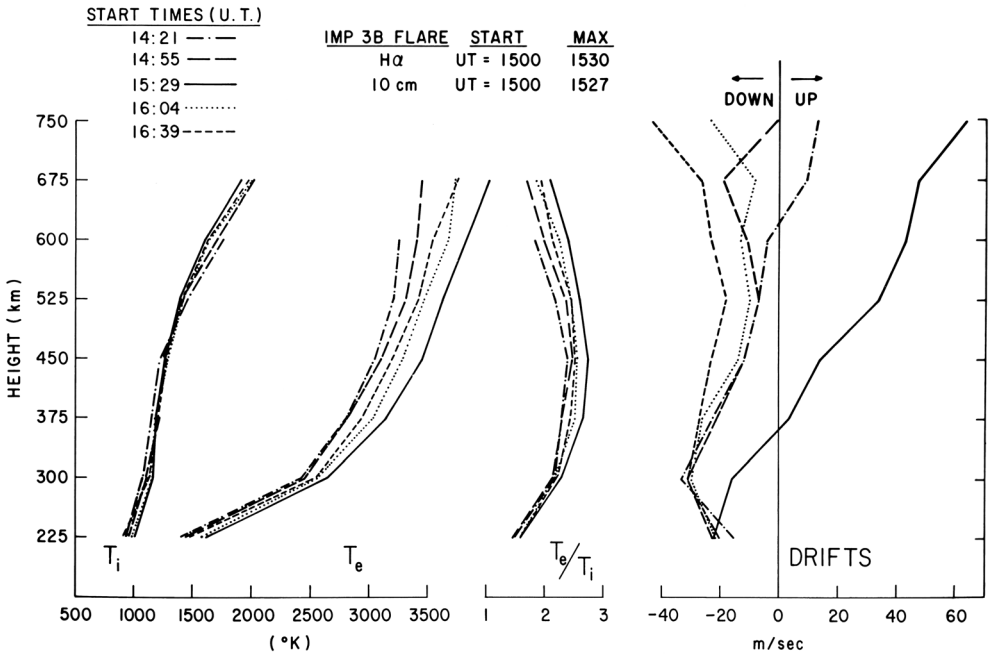

Figure 2. Millstone Hill incoherent scatter radar observations of ion temperatures, electron temperatures, and bulk plasma drifts versus height during the flare event depicted in Figure 1. Note that the profiles with the solid line pertain to peak flare times and show large enhancements in electron temperature and upward plasma drift (after Mendillo & Evans, 1974).

3. Flares in September 2017

September 2017 was a period of sustained solar activity with flares dominated by Active Region AR12673. On 6 September 2017, an X9.3 flare occurred near 11:53 UT (with peak emission near 12:02 UT and end time near 12:13 UT). Viewed from Earth, the active region was ~45°W from disk center. Four days later (10 September), an X8.2 flare occurred near 15:50 UT (with peak emission near 16:14 UT and end time near 16:51 UT). This same active region was near the limb as seen from Earth, but also observed at Mars by MAVEN's solar EUV Monitor (Eparvier et al., 2015). Ten days later (17 September), an M3.4 flare occurred near disk center, as viewed from Mars. The start time was near 11:45 UT and enhanced emission lasted for hours. Figure 3 provides the time histories of the four flares discussed in this paper (1972, 2017). Note that the reported flare times for the 7 August 1972 and 6 September 2017 flares correspond with when the flare irradiance reached Earth, whereas the reported flare times for the 10 and 17 September 2017 correspond with when the flare irradiance reached Mars. The difference in light travel time between the two planets is ~4 min.

For all four flare events, as anticipated, the pre-event (ambient) EUV fluxes are higher than the SXR magnitudes. The former account for the *F* layer at Earth and the M2-layer at Mars, while the latter produce the terrestrial *E* layer and the Martian M1-layer. The EUV patterns are the ones of interest for the topside ionosphere domains at both planets. As shown by the red curves in panels a and b, the two flares observed by the ISR at Millstone Hill are relatively similar with EUV peak values of ~5 mW/m^2. The major flare affecting Mars on 10 September 2017 shown in panel c is also one with maximum emission of ~5 mW/m^2, while the event of 17 September 2017 shown in panel d had fluxes of about half that value. The patterns for the September 2017 events in panels b and c have rapid rise and fall times in comparison to the more prolonged profile in panel d.

Enhanced solar fluxes cause multiple effects over different time spans. The sudden impact of more photons produces the equivalent of a solar maximum irradiance impacting a solar minimum neutral atmosphere. Large increases in photoionization produce large enhancements in electron densities. This initial phase lasts for perhaps 10–20 min depending on the time profile of the flare. Following this "early time" phase of solar photon absorption and ionization, the heated neutral atmosphere undergoes expansion. The solar irradiance continues to ionize the atmosphere now self-consistently in equilibrium with the Sun's output.

Flares also produce a population of solar energetic particles (SEPs) that travel at high speeds throughout the solar system. For Mars, with no global magnetic field to shield the atmosphere, collisions of SEPs and neutral

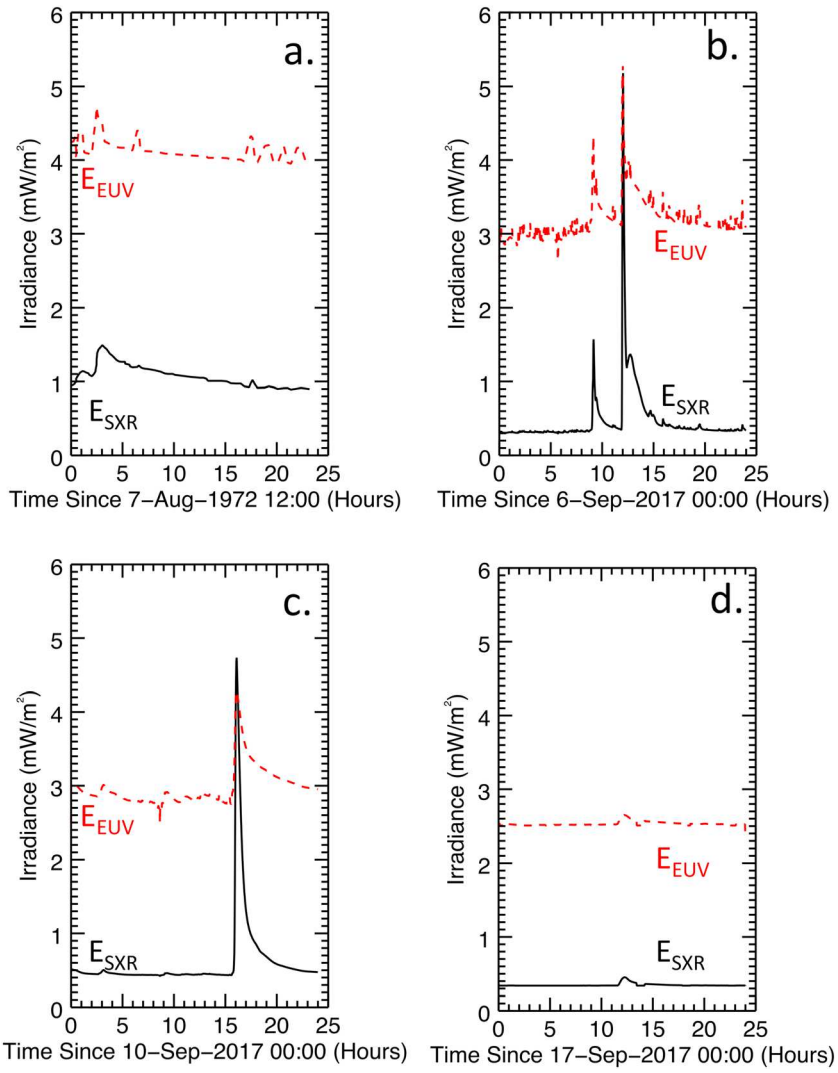

Figure 3. Solar X-ray (<100 A) and extreme ultraviolet (>100 A) wavelength-summed fluxes versus time for four events: 7 August 1972 to document a past event and 6, 10, and 17 September 2017 used in this study.

gases can add plasma to the ionosphere. Lillis and Fang (2015) have modeled such effects for a broad range of energetic particles. For the topic of interest here—the time span of flare photons producing ionization (tens of minutes to approximately an hour)—it is important to realize that the SEPs do not provide a second source function at "early times."As shown in Table 1 of Lee et al. (2018), SEP electrons arrived 3 hr after the peak flare time, and SEP ions arrived after two to three additional hours. Thus, the ionospheric flare effect at Mars treated here is the photon-atmosphere interaction only.

3.1. The 6 September 2017 Flare Effect at Earth

Figure 4 shows Earth ionospheric observations at midlatitudes from the Millstone Hill ISR on 6 September 2017 during the X9.3 class flare event that commenced at 11:53 UT. At the time, the radar was making vertical ionospheric observations with ~4 min temporal resolution using its 68 m zenith pointed antenna and a standard experiment mode providing *E* and *F* regions and near topside ionospheric information on a time-interleaved basis. *E* and *F* region measurements occurred at 36 km altitude resolution and 4.5 km altitude steps, and topside region measurements occurred at 144 km altitude resolution with 72 km altitude steps. For the results here, the *E* and *F* region data were further smoothed with a ~20 km wide low pass filter. The parameters in Figure 4 show *E* and *F* region electron density (bottom left) and electron temperature (bottom middle) at 100–350 km and topside region electron density (top left), electron temperature (top middle

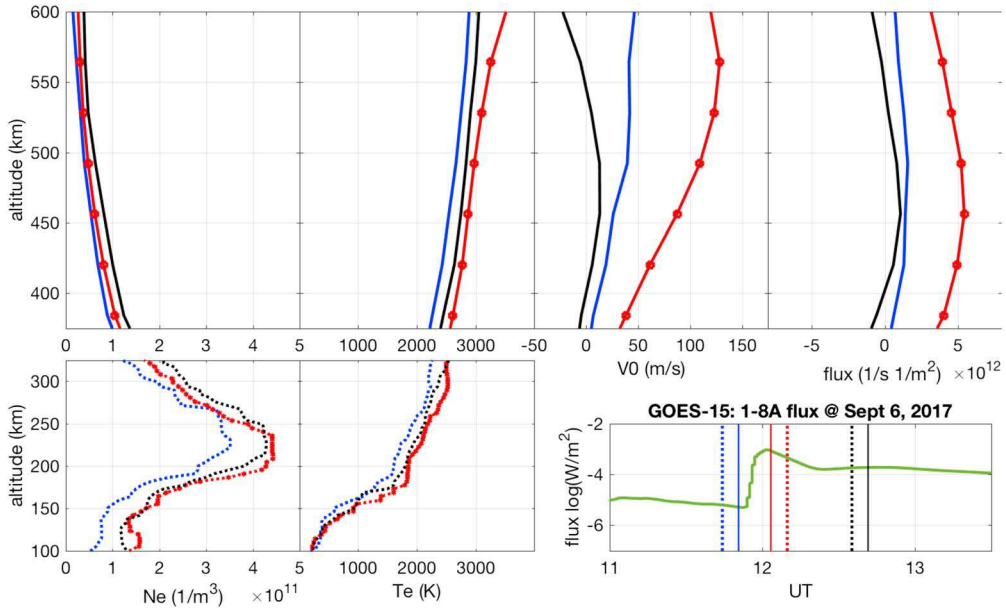

Figure 4. Millstone Hill observations of Earth ionospheric response during the X9 flare event at 11:53 UT on 6 September 2017. (bottom) *E* and *F* region measurements of (left) electron density and (middle) electron temperature at 100–350 km. (top) Topside ionosphere measurements of (left) electron density, (middle left) electron temperature, (middle right) vertical velocity, and (right) total ionospheric flux at 350–600 km. For each panel, preflare (blue), flare maximum (red), and postflare (black) curves are given, with dashed lines for *E*/*F* region profiles and solid lines for topside region profiles. (bottom right) 1–8 A solar flux as measured by the Geostationary Operational Environmental Satellite-15 spacecraft during 9–18 UT, with times of the three ionospheric topside profiles marked with corresponding colors and line styles.

left), vertical velocity (top middle right), and total ionospheric flux (top right) at 350–600 km. For each panel, preflare (blue), flare maximum (red), and postflare (black) curves are given, with dashed lines for *E*/*F* region profiles and solid lines for topside region profiles. The bottom right curve provides timing context for the Millstone Hill ionospheric profiles by showing 1–8 A solar flux as measured by the Geostationary Operational Environmental Satellite-15 spacecraft during 9–18 UT, with times of the three ionospheric topside profiles marked with corresponding colors and line styles.

As discussed above, there are two time scales for flare effects—a prompt ionization of the undisturbed upper atmosphere, followed by continued solar-induced ionization of the expanded atmosphere that results from flare heating. The effects of prompt ionization can clearly be seen in the enhanced flare maximum electron density curves throughout the entire ionosphere. Given that this flare occurred near sunrise, "late time" effects include both of these processes. Our emphasis, however, is upon the prompt response to flare onset above the *F* region peak. Figure 4 shows that the ambient positive (upward) drifts after sunrise experience a surge by nearly a factor of two at heights above 400 km, maximizing at and above 550 km altitude. The upward flare-induced flux maximizes near 450 km at 5–6 × 10^{14} ion-electron pairs/m^2/s and is associated with a ~400 K increase in electron temperature throughout the topside. While this is only the second time such effects have been reported in the literature using observations from Millstone Hill since 1972, the flare induced upward flux is unmistakable, and nearly the same as found for the 1972 solar flare described in Figures 1 and 2. While statistically limited, these case studies (as well as one for 7 September 2005; S. Zhang, private communication) suggest that an enhancement of upward plasma flux occurs for large flares observed at Earth.

3.2. September 2017 Flare Effects at Mars

Prior to the solar events of September 2017, MAVEN observations have documented the thermal expansion ("late phase") of the Martian thermosphere over a broad range of flare magnitudes (Thiemann et al., 2015). The altitudes of unit optical depth (i.e., the heights where ionospheric layers form) simply move upward with the expanding neutral atmosphere, resulting in weak (if any) plasma enhancements and lower electron temperatures due to cooling to CO_2. Thus, to observe the crucial initial phase of a flare's enhanced irradiance impacting the preflare atmosphere—when ionospheric densities and electron temperatures at fixed

heights are enhanced—observations are needed close to the flare maximum emission time that is typically in the first 10 min after flare onset. Due to MAVEN's highly elliptical orbit with a period of 4.5 hr, its presence within the ionosphere (~400 km inbound to periapse to ~400 km outbound) lasts for approximately 20 min. For this reason, there have been no published accounts of plasma changes within the ionosphere ($h < 400$ km) during the short initial phase of a flare. Faced with that observational gap, we report on models of flares at Earth (section 4) and then make a prediction of possible short-term effects at Mars (section 5). In section 6 we summarize MAVEN data sets from 10 and 17 September when ionospheric observations were made approximately 2 hr after each flare.

4. Model Results

Simulations of solar flare effects at Earth and Mars have concentrated on the altitudes where the greatest changes in electron density occur. These are the lower/secondary layers (*E* at Earth and M1 at Mars) where enhancements in soft X-rays produce far greater electron density increases (in percent) than those due to the EUV wavelengths that ionize the layers of maximum electron density (*F* at Earth and M2 at Mars). For Earth, Mendillo and Evans (1974) used a simple analytical model to relate the observed vertical drifts to electron temperature enhancements caused by the flare. To date, no advanced simulation code has been used to explore self-consistently the flare effects upon both electron densities and temperatures. Smithtro et al. (2006) used a time-dependent ionospheric model that had approximations and parameterizations for the secondary ionization and electron temperature enhancements caused by a sudden burst in photoelectrons during a flare. They succeeded in reproducing ionosonde and TEC signatures using the thermal expansion process to account for decreases in peak density while TEC was enhanced. No values of plasma drift speeds or upward fluxes of plasma were presented. A follow-up study by Sojka et al. (2013) used the same model with improved solar irradiance input to characterize flare effects in the lower ionosphere, with topside results similar to those in Smithtro et al. (2006). Using a fully numerical global model (TIME-GCM), Qian et al. (2010, 2011) conducted simulations of ionospheric enhancements (*E* layer and TEC) resulting from different locations of flares on the solar disk, as well as differences in flare rise and decay times. Results from these TIME-GCM model experiments dealt mainly with production and loss effects in the bottomside ionosphere. While TEC results were presented, minimal attention was given to changes in the topside ionosphere—only mentioning that "Contributions by electron transport processes were relatively weak."

For Mars, the flare simulations described by Lollo et al. (2012) dealt with photochemistry-only by eliminating plasma dynamics in the code described in Mendillo et al. (2011). Unfortunately, their results cannot offer quantitative insights into the transport issue raised here. As shown in their Figure 13, flare-induced plasma enhancements appeared in the topside ionosphere but, with plasma diffusion suppressed, the plasma was constrained to remain where it was produced. The photoelectrons created in the topside ionosphere would be expected to enhance electron temperatures—leading to an increase in upward diffusion and horizontal (day-to-night) plasma escape. Estimates of such a mechanism will be presented below.

In summary, simulations of plasma dynamics driven by flare-induced enhancements of electron density and electron temperature have never been modeled successfully at Earth, for example, by self-consistent simulations that reproduce the observed altitude profiles of N_e, T_e, and plasma velocities shown in Mendillo and Evans (1974). While plasma escape at Earth occurs during geomagnetic storms due to solar wind-magnetosphere-ionosphere coupling, it does not have a major evolutionary consequence to Earth as a planet. The situation is completely different at Mars. While there is no global magnetic field to hinder upward diffusing plasma at Mars, there are induced draped magnetic field lines that hinder vertical diffusion and, more importantly, redirect plasma flow to the antisunward (cross-terminator) direction. Solar flare induced modes of plasma escape—acting over billions of years—could be significant at Mars. They require a new and comprehensive approach to self-consistent modeling to determine how solar flares might have altered the Martian environment over billions of years.

5. Discussion and Estimates of Flare-Induced Upward Plasma Drifts

The consequence of a sudden appearance of solar photons at Earth is a phenomenon well known—the daily sunrise formation of the ionosphere. A solar flare provokes remarkably similar effects, but following a scenario that can occur suddenly at any point under daytime conditions. In effect, flares offer a "second sunrise" but in an exaggerated manner of magnitude and following a shorter time scale. At low altitudes, X-rays produce the

preflare *E* layer at 110 km and the diurnal pattern of its electron density follows changing solar zenith angles. Due to being embedded in a dense neutral atmosphere, there is no significant plasma transport and photoelectrons at those altitudes produce secondary ionization but do not modify thermal equilibrium ($T_e = T_i = T_n$). A solar flare simply follows the same scenario, adding to the preflare morphology of the *E* layer.

For the *F* layer at ~300 km, sunrise provokes a far more complicated scenario—and yet solar flares again offer an intense version of it. As sunrise occurs, photoelectrons collide with the remnant electrons of the nighttime (predawn) terrestrial ionosphere and raise their temperature. At the height of maximum electron density (N_mF_2), plasma diffusion competes with photochemistry and thus higher temperatures cause thermal expansion and enhanced diffusion (up and down). Most often, this reduces the value of N_mF_2 as plasma flows downward to regions of higher loss or upward into the topside ionosphere. Thus, the immediate effect of sunrise is a *decrease* in N_mF_2. This was initially called the *sunrise anomaly* until the full explanation was known (see Evans, 1968, and references therein). Flares often cause the same scenario—that is, while the *E* layer is enhanced, the *F* layer shows a small decrease in electron density (Handzo et al., 2014). This does not always occur, probably depending on the flare location on the solar disk (Handzo et al., 2014). For the cases shown in Figures 1 and 4, there were increases in N_mF_2. The key point of interest here is not the response in N_mF_2 but the enhanced electron temperatures at higher altitudes that drive upward drift.

Evans (1971) presented a simple model of how plasma temperatures affect ionospheric drifts in the Earth's topside ionosphere. It was assumed that above some reference level (z_o) production and loss of plasma are negligible, the ion composition is O^+, the plasma temperature ($T_e + T_i$) is constant with height, and the topside electron density can be represented using the hydrostatic equilibrium (exponential with scale height) law. These are reasonable approximations for the daytime ionosphere. If the plasma temperatures increase at a constant rate with time, the plasma scale height [$H = k\,(T_e + T_i)/m_i g$] changes as dH/dt = constant; if the density at the reference level also changes at a constant rate, then dN_o/dt = constant. Evans (1971) showed that for hydrostatic equilibrium to be maintained under these changes, there must be a flux of plasma through z_o, with the vertical velocity given by

$$V_z = (H/N_o)\, dN_o/dt \;+\; [1 + (z - z_o)/H]\, dH/dt \tag{1}$$

Mendillo and Evans (1974) referred to the first quantity as the "pressure term" and the second as the "thermal term"—the first providing a constant value, while the second gave values that increased with altitude. They showed that the altitude dependence of observed vertical drift shown in Figure 1 was well represented by the second term in equation (1), using observations to determine z_o = 525 km, H = 300 km, Δh = 25 km, and Δt = 600 s. Figure 4 results for the 6 September 2017 solar flare follow this same scenario.

What might equation (1) say about flare effects at Mars? Evans (1971) addressed the case of vertical plasma diffusion (equivalent to no B field or one that is vertical). For Mars, as described above, vertical plasma diffusion operates to the point where draped B lines hinder flow and redirect dynamics from vertical to horizontal. This occurs in the topside ionosphere and, for the estimates to be made here, we will assume that flare-induced vertical fluxes ultimately become horizontal escape fluxes.

To address the topic, we use the simulation results for $N_e(h)$, $T_e(h)$, and $T_i(h)$ described in Matta et al. (2014) for the Martian preflare ionosphere (heights between 80 and 400 km). The model runs were conducted for the solar minimum conditions appropriate for the Viking-1 descent probes that provided the first in situ observations of those quantities at Mars (Hanson et al., 1977; Hanson & Mantas, 1988; Mayyasi & Mendillo, 2015). From Figures 8 and 9 in Matta et al. (2014), we extract the following values:

$$z_o = 200 \text{ km}$$
$$N_o = 1\times10^{10} e^-/m^3$$
$$T_e = 4000 \text{ K}$$
$$T_i = 2000 \text{ K}$$
$$m_i(O_2^+) = 53.4\times10^{-27} \text{ kg}$$
$$g = 3.8 \text{ m/s}^2$$
$$k = 1.381\times10^{-23} \text{ J/K}$$
$$H = 400 \text{ km}$$

Table 1
Preflare and Postflare Orbit Summary

	10 September 2017		17 September 2017	
Preflare orbits	5716 (inbound)	13:06–13:16 (UT)	5753 (inbound)	09:10–09:20 (UT)
	5717 (outbound)	13:16–13:26 (UT)	5754 (outbound)	09:20–09:29 (UT)
Flare onset	15:50 (UT)		11:45 (UT)	
Postflare orbits	5717 (inbound)	17:32–17:42 (UT)	5754 (inbound)	13:36–13:46 (UT)
	5718 (outbound)	17:42–17:52 (UT)	5755 (outbound)	13:46–13:55 (UT)
ΔTime from flare onset to periapse	1 hr 52 min		2 hr 1 min	

For a flare that increases the electron density at z_o by 10% ($\Delta N_o = 1 \times 10^9$ e$^-$/m^3) in 10 min (Δt = 600 s), the pressure term in equation (1) gives V_z = 67 m/s for the velocity independent of altitude. For the altitude-dependent second term in equation (1), if the electron temperature increased from a constant value of 4,000 to 5,000 K in 600 s, the following values occur for V_z: 114 m/s at 200 km, 143 m/s at 300 km, 157 m/s at 350 km, and 171 m/s at 400 km. The upward flux of O_2^+ at 350 km (Flux = $N_e \times V_z$) for the Viking-1 simulation was 2.4×10^{11} ions/m^2/s (from 3×10^9 e$^-$/m$^3 \times$ 80 m/s)—a value we use to portray the preflare estimate. Using a 10% increase in electron density at 350 km due to the flare, and the vertical speed of 157 m/s calculated for that altitude for the thermal term, the flux at 350 km becomes 5.2×10^{11} ions/m^2/s (3.3×10^9 e$^-$/m$^3 \times$ 157 m/s). This rough calculation thus suggests that a flare can double the escape of plasma over the dayside ionosphere of Mars—for at least the duration of the flare's most active period (10–20 min). Integrated over the full dayside (hemispheric) surface area at the top of the Martian ionosphere (~10^{14} m^2), the total plasma escape rate is ~5×10^{25}/s. This is a factor of 10 higher than plasma escape rates quoted in the introduction, but of course its impact is only for tens of minutes. Over a four billion year period of solar flares, however, it is perhaps not a minor contributor to escape, and especially so where the Sun was far more active early in the solar system's history.

6. What Did MAVEN Observe?

We now summarize the ionospheric observations made by the Langmuir Probe and Wave (LPW) instrument onboard the MAVEN satellite during the two flare events of September 2017. At flare onset on 10 September 2017 (15:50 UT), MAVEN was at an altitude of 5,937 km and thus well beyond the ionosphere. On 17 September 2017, flare onset was at 11:45 UT, and MAVEN was again near apoapse altitudes (6,047 km). Prior to both flares, there were observations within the ionosphere that we use as control curves for judging postflare observations made on the subsequent orbit. The orbits and times of these observations are given in Table 1 (noting that orbit numbers change at periapse, and "in ionosphere" is taken to be below 400 km).

MAVEN observations within the ionosphere thus relate to solar flare "late times" as defined above. Figure 5 shows the temporal relationships between altitude and solar zenith angles for these orbits. For each event, the top panel shows MAVEN's orbital altitude versus time using a dashed line. The time of the flare is marked by a solid dot, and the time span within the ionosphere ($h < 400$ km) is shown by the heavy shading of the trajectory. The lower panels show solar zenith angles using the same format.

The high solar zenith angle domains shown in Figure 5 are the ones usually associated with radio occultation experiments. If early time observations within the ionosphere had been possible by MAVEN, anticipated flare effects would have been similar to those documented in previous radio occultation experiment studies (Fallows et al., 2015; Mahajan, 2009; Mendillo et al., 2006). A major difference, however, is that occultation experiments sample a small range of latitudes and longitudes during a short time period. During the ~20 min that MAVEN spent below 400 km on each of the orbits shown above, a rather large latitude range was sampled (see Table S1 in the supporting information). Given this coverage, and the fact that flares impact the entire dayside hemisphere, we decided to average the inbound and outbound observations of electron densities and electron temperatures to obtain single preflare and postflare ionospheric profiles. The results are shown in Figure 6.

The LPW observations of electron density (N_e) and electron temperature (T_e) below 400 km, taken before and after the strong flare of 10 September 2017, reveal two signatures. The ionospheric patterns below ~225 km

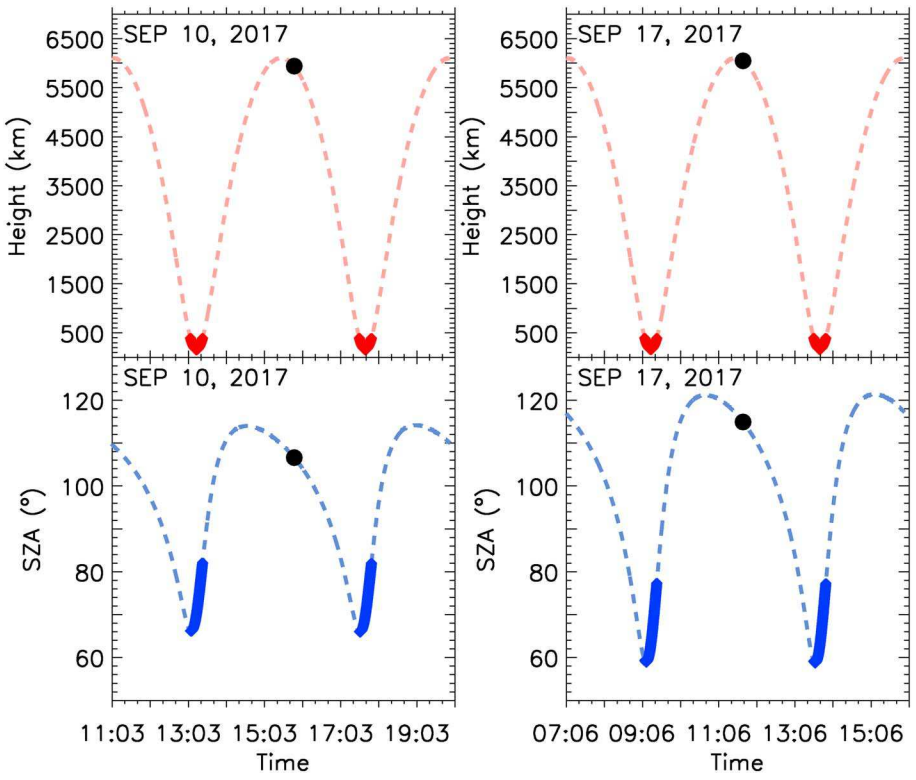

Figure 5. (top row) The positions of the MAVEN spacecraft during the solar flare events of 10 and 17 September 2017. The dashed lines give altitude versus time, with the dots near periapse indicating the times of flares, and the shading indicates times when the spacecraft was below 400 km. (bottom row) The variation in solar zenith angles during the orbits shown above. At the time of the flare on 10 September 2017, MAVEN was at 5,937 km, latitude = 59.1°S, longitude = 136.3°E, and solar zenith angle (SZA) = 106.6°. For the 17 September flare, MAVEN was at height = 6,047 km, latitude = 49.9°S, longitude = 246.6°E, and SZA = 114.9°. During periapse passage, MAVEN sampled SZAs between ~65° and 83° (10th) and ~58°–78° (17th).

exhibit the "late flare" scenario described earlier (Thiemann et al., 2015) and contemporaneously by several authors dealing with this September 2017 period (e.g., Jain et al., 2018; Lee et al., 2018; Thiemann et al., 2018). Enhancements at fixed heights are due to ionization of the expanded neutral atmosphere, and reduced T_e values are due to enhanced cooling to the higher CO_2 densities at those heights. Here we focus on higher altitudes. Between 300 and 400 km, depletions in N_e are observed, and they are associated with elevated T_e values. Is this a signature of plasma escape driven by elevated plasma temperatures so long after the flare? Possibly, but unlikely. The pattern above 300 km is certainly the opposite of that found at lower heights ($h < 225$ km). Yet the cooling process for electrons itself varies with height from energy loss to neutrals at low altitudes to other means (e.g., cooling to ions to neutrals) in a topside ionosphere (Schunk & Nagy, 2009). Thus, at low altitudes N_e and T_e are anticorrelated due to neutrals, while high in the topside ionosphere N_e and T_e are anticorrelated due to plasma heat sharing processes.

The $T_e(h)$ profile in Figure 6 (top right) for preflare conditions appears typical—with a strong positive gradient to ~200 km merging to a near constant value above. The postflare $T_e(h)$ profile has the strong gradient at low altitudes continue to ~300 km where reduced N_e values appear with higher T_e values. Guided by the results in Figure 6 for preflare conditions, it is possible to estimate the type of dynamics possible by use of equation (1). For input conditions, we adopted z_o = 200 km, $N_o = 6 \times 10^9$ e^-/cm^3, T_e = 2,000 K, and T_i (assumed) = 1,000 K. If the flare caused a 10% increase in N_o, and T_e to increase by 1,000 K, the resultant upward drifts would be 34 m/s for the thermal term and 114 to 225 m/s for drifts between 200 and 400 km. Unfortunately, these are no plasma drift observations available to compare with such estimates.

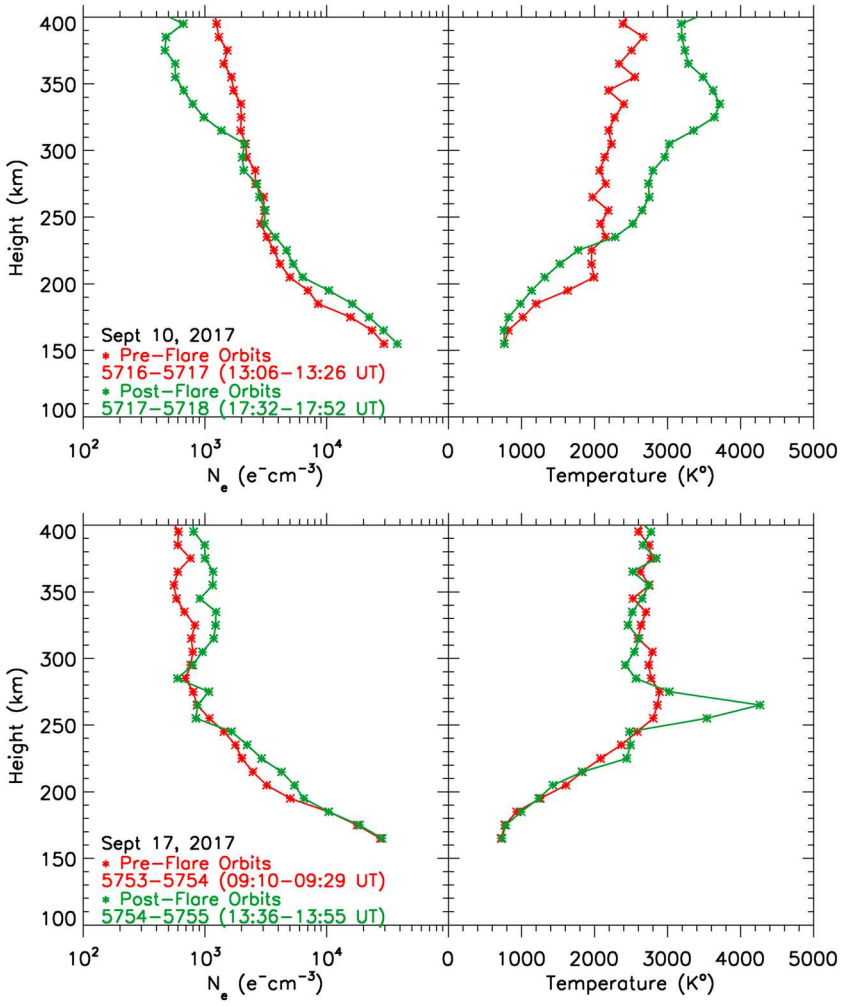

Figure 6. Observations by MAVEN's Langmuir Probe and Waves instrument on the days of (top) 10 September 2017 and (bottom) 17 September 2017. Electron densities are on the left and electron temperatures on the right. Averages of the inbound and outbound observations for the preflare periapse pass below 400 km are shown by red symbols, while those for the postflare passes are in green. All symbols represent 10-km averages. The spikes in T_e and N_e at ~270 km on 17 September (lower panels) are reliable data points, but effects not related to photon flux enhancements.

Equally unfortunate is that turning to the 17 September data set (lower panels of Figure 6) sheds no additional light on the problem. As shown in Figure 3, this was a less energetic flare and the LPW data in the lower panels of Figure 6 exhibit no changes from preflare conditions below 200 km, and virtually none above.

We integrated the MAVEN $N_e(h)$ profiles shown in Figure 6 and found the following changes in the TEC from periapse to 400 km (using TEC units of 10^{15} e^-/m^2): 1.5 to 1.7 TECU on 10 September 2017 and 0.9 to 1.1 TECU on 17 September 2017. These are not complete TEC values since they do not include the portions of the ionosphere below ~150 km (including the peak electron density). For solar zenith angles in the range 65°–85° during average solar flux conditions of September 2017, the Mars Initial Reference Ionosphere model (http://sirius.bu.edu/miri/) gives full TEC values in the range 2.5 to 4.5 TECU, as derived using observations from the SHARAD radar on the MRO spacecraft (Mendillo, Narvaez, Campbell 2017). No evidence for TEC enhancements at late times can be drawn from these observations.

Finally, we note that there was a previous, relatively weak M-class flare that occurred close to a time when MAVEN was within the ionosphere (24 March 2015, as described in Thiemann et al., 2015). Due to spacecraft operational reasons, the solar irradiance profile was incomplete and thus early versus late time ionospheric effects cannot be identified. For completeness, the available solar and LPW data are shown in the Supporting Information.

7. Summary

We have investigated the possibility of ionospheric enhancements and upward plasma dynamics due to solar flares being a candidate contributor to plasma escape at Mars. A solar active region in September 2017 produced flares that impacted the Earth's ionosphere on 6 September, and then the Martian ionosphere on 10 and 17 September. On Earth, where flare effects upon the ionosphere are well documented, past observations showed a surge in upward plasma drift of flare-induced electron density enhancements driven by increases in electron temperature. The consistency of that pattern was again observed from observations on 6 September by the Millstone Hill ISR. The locations of the MAVEN spacecraft at the times of the flares on 10 and 17 September were at heights of ~6,000 km and thus well above the ionosphere where "early time" flare effects could not be observed. Ionospheric data taken below 400 km became available 2 hr after the flares and show possible signs of lingering flare effects—with the stronger flare event of 10 September being the more likely candidate. Estimates of the magnitudes of flare-induced upward drifts (and escape rates) at Mars were made using a model validated by terrestrial observations, and the results suggest significant escape possibilities. In section 5, for example, using equation (1) with simulation values appropriate for the Viking-1 conditions, the estimate for the flare scenario at Mars resulted in the "pressure term" constant upward speed value of 67 m/s, with the altitude dependent "thermal term" speeds ranging from 114 m/s at 200 km to 171 m/s at 350 km. For the 10 September 2017 conditions in Figure 6, the equation (1) simulation estimates were 34 m/s for the pressure term and 114–225 m/s (200–400 km) for the thermal term. The electron densities at 350 km were 3×10^3 e^-/cm^3 for Viking simulations (Figure 8 in Matta et al., 2014) and 2×10^3 e^-/cm^3 for the MAVEN case (Figure 6, upper left). Thus, use of equation (1) for estimates of upward speeds had comparable Viking-MAVEN background values.

No published model of the Martian ionosphere has self-consistently simulated the overall scenario of solar flare effects, and in particular the electron temperature changes that could provoke the early time escape effects predicted in our study. Hopefully, that situation will change and new flare events (with X-class magnitudes) will be observed by MAVEN instruments while within the ionosphere, allowing for tests of the mechanism proposed here.

Acknowledgments
At Boston University, this work was supported, in part, by contract funds from the NASA MAVEN mission, the NSF INSPIRE program for comparative ionospheres AST-1545581, the NSF Aeronomy Program AGS-1659304, and resources provided through the Center for Space Physics. Radar observations and analysis at Millstone Hill are supported by Cooperative Agreement AGS-1242204 between the National Science Foundation and the Massachusetts Institute of Technology. The MAVEN data are available to the public through the Planetary Plasma Interactions node of NASA's Planetary Data System, at https://pds-ppi.igpp.ucla.edu/. Radar data access is available through the Madrigal Database at Haystack Observatory at http://madrigal.haystack.mit.edu/madrigal/. Geostationary Operational Environmental Satellite-15 data can be accessed via NOAA's National Center for Environmental Information (https://www.ngdc.noaa.gov/stp/satellite/goes/dataaccess.html).

References

Banks, P., & Kockarts, G. (1973). *Aeronomy*. New York: Academic Press.
Barabash, S., Fedorov, A., Lundin, R., & Sauvaud, J.-A. (2007). Martian atmospheric erosion rates. *Science*, *315*(5811), 501–503. https://doi.org/10.1126/science.1134358
Brain, D., McFadden, J. P., Halekas, J. S., Connerney, J. E. P., Bougher, S. W., Curry, S., et al. (2015). The spatial distribution of planetary ion fluxes near Mars observed by MAVEN. *Geophysical Research Letters*, *42*, 9142–9148. https://doi.org/10.1002/2015GL065293
Catling, D., & Kasting, J. (2017). *Atmospheric evolution on inhabited and lifeless worlds*. Cambridge, UK: Cambridge University Press.
Dong, Y., Fang, X., Brain, D. A., McFadden, J. P., Halekas, J. S., Connerney, J. E., et al. (2015). Strong plume fluxes at Mars observed by MAVEN: An important planetary ion escape channel. *Geophysical Research Letters*, *42*, 8942–8950. https://doi.org/10.1002/2015GL065346
Dubinin, E., Fraenz, M., Woch, J., Barabash, S., & Lundin, R. (2009). Long-lived auroralstructures and atmospheric losses through auroral flux tubes on Mars. *Geophysical Research Letters*, *36*, L08108. https://doi.org/10.1029/2009GL038209
Eparvier, F., Chamberlin, P., Woods, T., & Thiemann, E. (2015). The solar extreme ultraviolet monitor for MAVEN. *Space Science Reviews*, *195*(1-4), 293–301. https://doi.org/10.1007/s11214-015-0195-2
Evans, J. V. (1968). Sunrise behavior of the F layer at midlatitudes. *Journal of Geophysical Research: Space Physics*, *73*, 3489–3504. https://doi.org/10.1029/JA073i011p03489
Evans, J. V. (1969). Theory and practice of ionosphere study by Thomson scatter radar. *Proceedings of the IEEE*, *57*(4), 496–530. https://doi.org/10.1109/PROC.1969.7005
Evans, J. V. (1971). Observations of F region vertical velocities at Millstone Hill, 1. Evidence for drifts due to expansion, contraction, and winds. *Radio Science*, *6*, 609–626. https://doi.org/10.1029/RS006i006p00609
Fallows, K., Withers, P., & Gonzales, G. (2015). Response of the Mars ionosphere to solar flares:Analysis of MGS radio occultation data. *Journal of Geophysical Research: Space Physics*, *120*, 9805–9825. https://doi.org/10.1002/2015JA021108
Foster, J. C., Coster, A. J., Erickson, P. J., Rich, F. J., & Sandel, B. R. (2004). Stormtime observations of the flux of plasmaspheric ions to the dayside cusp/magnetopause. *Geophysical Research Letters*, *31*, L08809. https://doi.org/10.1029/2004GL020082
Fränz, M., Dubinin, E., Nielsen, E., Woch, J., Barabash, S., Lundin, R., & Fedorov, A. (2010). Transterminator ion flow in the Martian ionosphere. *Planetary and Space Science*, *58*(11), 1442–1454. https://doi.org/10.1016/j.pss.2010.06.009
Garriott, O., daRosa, A., Mavis, M., & Villard, O. Jr. (1967). Solar flare effects in the ionosphere. *Journal of Geophysical Research*, *72*, 6099–6103. https://doi.org/10.1029/JZ072i023p06099
Gurnett, D., Kirchner, D. L., Huff, R. L., Morgan, D. D., Persoon, A. M., Averkamp, T. F., et al. (2005). Radar soundings of the ionosphere of Mars. *Science*, *310*(5756), 1929–1933. https://doi.org/10.1126/science.1121868
Handzo, R., Forbes, J., & Reinisch, B. (2014). Ionospheric electron density response to solar flares as viewed by digisondes. *Space Weather*, *12*, 205–216. https://doi.org/10.1002/2013SW001020
Hanson, W., & Mantas, G. (1988). Viking electron temperature measurements: Evidence of a magnetic field in the Martian ionosphere. *Journal of Geophysical Research*, *93*, 7538–7544. https://doi.org/10.1029/JA093iA07p07538

Hanson, W., Santatani, S., & Zuccaro, D. (1977). The Martian ionosphere as observed by the Viking Retarding Potential Analyzers. *Journal of Geophysical Research*, *82*, 4351–4363. https://doi.org/10.1029/JS082i028p04351

Jain, S. K., Deighan, J., Schneider, N. M., Stewart, A. I. F., Evans, J. S., Thiemann, E. M. B., et al. (2018).Martian thermospheric response to an X8.2 solar flare on September 10, 2017 as seen by MAVEN/IUVS. *Geophysical Research Letters*, *45*. https://doi.org/10.1029/2018GL077731

Jakosky, B. (2015). MAVEN explores the Martian upper atmosphere. *Science*, *350*(6261), 643. https://doi.org/10.1126/science.aad3443

Jakosky, B., Grebowsky, J., Luhmann, J., Connerney, J., Eparvier, F., Ergun, R., et al. (2015).MAVEN observations of the response of Mars to an interplanetary coronal mass ejection.*Science*, *350*(6261), aad0210. https://doi.org/10.1126/science.aad0210

Lee, C. O., Jakosky, B. M., Luhmann, J. G., Brain, D. A., Mays, M. L., Hassler, D. M., et al. (2018). Observations and Impacts of the 10 September 2017 Solar Events at Mars: An Overview and Synthesis of the Initial Results, *Geophysical Research Letters*, *45*. https://doi.org/10.1029/2018GL079162

Lillis, R., & Fang, X. (2015). Electron impact ionization in the Martian ionosphere: Interplay between scattering and crustal magnetic field effects. *Journal of Geophysical Research: Planets*, *120*, 1332–1345. https://doi.org/10.1002/2015JE004841

Lollo, A., Withers, P., Fallows, K., Girazian, Z., Matta, M., & Chamberlin, P. (2012). Numericalsimulations of the ionosphere of Mars during a solar flare. *Journal of Geophysical Research*, *117*, A05314. https://doi.org/10.1029/2011JA017399

Lundin, R., Barabash, S., Fedorov, A., Holmström, M., Nilsson, H., Sauvaud, J.-A., & Yamauchi, M. (2008). Solar forcing and planetary ion escape from Mars. *Geophysical Research Letters*, *35*, L09203. https://doi.org/10.1029/2007GL032884

Lundin, R., Barabash, S., Holmström, M., Nilsson, H., Yamauchi, M., Dubinin, E. M., & Fraenz, M. (2009). Atmospheric origin of cold ion escape from Mars. *Geophysical Research Letters*, *36*, L17202. https://doi.org/10.1029/2009GL039341

Lundin, R., Hultqvist, B., Olsen, S., Pellinen, R., Liede, I., Zakharov, A., et al. (1989). The ASPERA experiment on the Soviet Phobos spacecraft. In J. H. Waite, Jr., J. L. Burch, & R. L. Moore (Eds.), *Solar system plasma physics,* geophysics monogram series (Vol. 54, pp. 417–424). Washington, DC: American Geophysical Union. https://doi.org/10.1029/GM054p0417

Mahajan, K., Lodhi, N., & Singh, S. (2009). Ionospheric effects of solar flares at Mars. *Geophysical Research Letters*, *36*, L15207. https://doi.org/10.1029/2009GL039454

Matta, M., Galand, M., Moore, L., Mendillo, M., & Withers, P. (2014). Numerical simulations of ion and electron temperature in the ionosphere of Mars: Multiple ions and diurnal variations. *Icarus*, *227*, 78–88. https://doi.org/10.1016/j.icarus.2013.09.006

Mayyasi, M., & Mendillo, M. (2015). Why the Viking descent probes found only one ionospheric layer at Mars. *Geophysical Research Letters*, *42*, 7359–7365. https://doi.org/10.1002/2015GL065575

Mendillo, M., & Evans, J. (1974). Incoherent scatter observations of the ionospheric response to a large solar flare. *Radio Science*, *9*, 197–203. https://doi.org/10.1029/RS009i002p00197

Mendillo, M., Klobuchar, J. A., Fritz, R. B., da Rosa, A. V., Kersley, L., Yeh, K. C., et al. (1974). Behavior of the ionospheric F region during the great solarflare of August 7, 1972. *Journal of Geophysical Research*, *79*, 665–672. https://doi.org/10.1029/JA079i004p00665

Mendillo, M., Lollo, A., Withers, P., Matta, M., Pätzold, M., & Tellmann, S. (2011). Modeling Mars' ionosphere with constraints from same-day observations by Mars Global Surveyor and Mars Express. *Journal of Geophysical Research*, *116*, A11303. https://doi.org/10.1029/2011JA016865

Mendillo, M., Narvaez, C., & Campbell, B. (2017). The total electron content of the Martian ionosphere from MRO/SHARAD observations. *Ionospheric response to the X*, *122*, 2182–2192. https://doi.org/10.1002/2017JE005391

Mendillo, M., Narvaez, C., Vogt,M. F., Mayyasi, M., Mahaffy, P., Benna, M., et al. (2017).MAVEN and the total electron content of the Martian ionosphere. *Journal of Geophysical Research: Space Physics, 122,* 3526–3537. https://doi.org/10.1002/2016JA023474

Mendillo, M., Withers, P., Hinson, D., Rishbeth, H., & Reinisch, B. (2006). Effects of solar flares on the ionosphere of Mars. *Science*, *311*(5764), 1135–1138. https://doi.org/10.1126/science.122099

Mitra, A. (1974). *Ionospheric effects of solar flares*. Boston, MA: D. Reidel.

Nielsen, E., Zou, H., Gurnett, D. A., Kirchner, D. L., Morgan, D. D., Huff, R., et al. (2006). Observations of vertical reflections from the topside Martian ionosphere. *Space Science Reviews*, *126*(1-4), 373–388. https://doi.org/10.1007/s11214-006-9113-y

Nilsson, H., Carlsson, E., Brain, D., Yamauchi, M., Holmström, M., Barabash, S., et al. (2010). Ion escape from Mars as a function of solar wind conditions: A statistical study. *Icarus*, *206*(1), 40–49. https://doi.org/10.1016/j.icarus.2009.03.006, 2010

Nilsson, H., Edberg, N. J. T., Stenberg, G., Barabash, S., Holmström, M., Futaana, Y., et al. (2011). Heavy ion escape from Mars, influence from solar wind conditions and crustal magnetic fields. *Icarus*, *215*(2), 475–484. https://doi.org/10.1016/j.icarus.2011.08.003

Peterson, W. K., Collin, H. L., Yau, A. W., & Lennartsson, O. W. (2001). Polar/toroidal imaging mass-angle spectrograph observations of suprathermal ion outflow during solar minimum conditions. *Journal of Geophysical Research*, *106*, 6059–6066. https://doi.org/10.1029/2000JA003006

Peterson, W. K., Thiemann, E. M. B., Eparvier, F. G., Andersson, L., Fowler, C. M., Larson, D., et al. (2016). Photoelectrons and solar ionizing radiation at Mars: Predictions versus MAVEN observations. *Journal of Geophysical Research: Space Physics*, *121*, 8859–8870. https://doi.org/10.1002/2016JA022677

Qian, L., Burns, A., Chamberlin, P., & Solomon, S. (2010). Flare location on the solar disk: Modeling the thermosphere and ionosphere response. *Journal of Geophysical Research*, *115*, A09311. https://doi.org/10.1029/2009JA015225

Qian, L., Burns, A., Chamberlin, P., & Solomon, S. (2011). Variability of thermosphere and ionosphere response to solar flares. *Journal of Geophysical Research, 116*, A10309. https://doi.org/10.1029/2011JA016777

Ramstad, R., Futaana, Y., Barabash, S., Nilsson, H., del Campo, B., M, S., et al. (2013). Phobos 2/ASPERA data revisited: Planetary ion escape rate from Mars near the 1989 solar maximum. *Geophysical Research Letters*, *40*, 477–481. https://doi.org/10.1002/grl.50149

Rishbeth, H., Mendillo, M., Wroten, J., & Roble, R. (2009). Day-to-day modelling of the ionospheric F2-layer for year 2002. *Journal of Atmospheric and Solar-Terrestrial Physics*, *71*(8-9), 848–856. https://doi.org/10.1016/j.jastp.2009.03.022

Roble, R., & Ridley, E. (1994). A thermosphere-ionosphere-mesosphere-electrodynamics general circulation model (TIME-GCM): Equinox solar cycle minimum simulations (30-500 km). *Geophysical Research Letters*, *21*, 417–420. https://doi.org/10.1029/93GL03391

Sandel, B. R., & Denton, M. H. (2007). Global view of refilling of the plasmasphere. *Geophysical Research Letters*, *34*, L17102. https://doi.org/10.1029/2007GL030669

Schunk, R., & Nagy, A. (2009). *Ionospheres: Physics, plasma physics, and chemistry* (2nd ed.). Cambridge: Cambridge University Press.

Smithtro, C., Sojka, J., Berkey, T., Thompson, D., & Schunk, R. (2006). Anomalous F region response to moderate solar flares. *Radio Science*, *41*, RSs5S03. https://doi.org/10.1029/2005RS003350

Sojka, J., Jensen, J., David, M., Schunk, R., Woods, T., & Eparvier, F. (2013). Modeling the ionospheric E and F1 regions: Using SDO-EVE observations as the solar irradiance driver. *Journal of Geophysical Research: Space Physics*, *1118*, 5379–5391. https://doi.org/10.1002/jgra.50480

Strangeway, R. J., Ergun, R. E., Su, Y.-J., Carlson, C. W., & Elphic, R. C. (2005). Factors controlling ionospheric outflows as observed at intermediate altitudes. *Journal of Geophysical Research*, *110*, A03221. https://doi.org/10.1029/2004JA010829

Strangeway, R. J., Russell, C. T., Luhmann, J. G., Moore, T. E.,Foster, J. C., Barabash, S. V.&Nilsson,H. (2010).Does a planetary-scale magnetic field enhance or inhibit ionospheric plasma outflows? Abstract SM33B-1893.Fall AGU Meeting, San Francisco, December 13-17, 2010.

Thiemann, E. M. B., Andersson, L., Lillis, R., Withers, P., Xu, S., Elrod, M., et al. (2018). The Mars topside ionosphere response to the X8.2 solar flare of 10 September 2017. *Geophysical Research Letters*, *45*. https://doi.org/10.1029/2018GL077730

Thiemann, E. M. B., Eparvier, F. G., Andersson, L. A., Fowler, C. M., Peterson, W. K., Mahaffy, P. R., et al. (2015). Neutral density response to solar flares at Mars. *Geophysical Research Letters*, *42*, 8986–8992. https://doi.org/10.1002/2015GL066334

Thome, G., & Wagner, L. (1971). Electron density enhancements in the E and F regions of the ionosphere during solar flares. *Journal of Geophysical Research*, *76*, 6883–6895. https://doi.org/10.1029/JA076i028p06883

Tsurutani, B. T., Verkhoglyadova, O. P., Mannucci, A. J., Lakhina, G. S., Li, G., & Zank, G. P. (2009). A brief review of "solar flare effects" on the ionosphere. *Radio Science*, *44*, RS0A17. https://doi.org/10.1029/2008RS004029

Xiong, B., Wan, W., Liu, L., Withers, P., Zhao, B., Ning, B., et al. (2011). Ionospheric response to the X-class solar flare on 7 September 2005. *Journal of Geophysical Research*, *116*, A11317. https://doi.org/10.1029/2011JA016961

Yau, A. W., Shelley, E. G., Peterson, W. K., & Lenchyshyn, L. (1985). Energetic auroral and polar ion outflow at DE 1 altitudes: Magnitude, composition, magnetic activity dependence, and long-term variations. *Journal of Geophysical Research*, *90*, 8417–8432. https://doi.org/10.1029/JA090iA09p08417